Steady State Analysis of Small Molten Salt Reactor*
(Effect of Fuel Salt Flow on Reactor Characteristics)

Takahisa YAMAMOTO**, Koshi MITACHI** and Takashi SUZUKI**

The Molten Salt Reactor (MSR) is a thermal neutron reactor with graphite moderation and operates on the thorium-uranium fuel cycle. The feature of the MSR is that fuel salt flows inside the reactor during the nuclear fission reaction. In the previous study, the authors developed numerical model with which to simulate the effects of fuel salt flow on the reactor characteristics. In this study, we apply the model to the steady-state analysis of a small MSR system and estimate the effects of fuel flow. The model consists of two-group neutron diffusion equations for fast and thermal neutron fluxes, transport equations for six-group delayed neutron precursors and energy conservation equations for fuel salt and the graphite moderator. The following results are obtained: (1) in the rated operation condition, the peaks of the neutron fluxes slightly move toward the bottom from the center of the reactor and the delayed neutron precursors are significantly carried by the fuel salt flow, and (2) the extension of residence time in the external-loop system and the rise of the fuel inflow temperature show weak negative reactivity effects, which decrease the neutron multiplication factor of the small MSR system.

***Key Words*:** Molten Salt Reactor, Delayed Neutron Precursor, Fuel Salt Flow, Neutron Flux

1. Introduction

In the thorium (Th) - uranium (U) fuel cycle, Th transmutes to an excellent fuel for nuclear reactors, the fissile ^{233}U, when Th absorbs one neutron. Such a fuel cycle has two important features: (1) fissile ^{233}U generates negligible amounts of plutonium (Pu) and minor actinides, and (2) Th is abundant on the earth, existing in about 3–4 times the reserves of natural uranium. Hence the Th-U fuel cycle will become an important energy resource in the near future. One of the reactors suitable for utilizing the Th-U fuel cycle is the molten salt reactor (MSR), which is a thermal neutron reactor with graphite moderation. Conventional nuclear reactors, such as the boiling-water reactor (BWR) and the pressurized-water reactor (PWR), use solid nuclear fuels, but the MSR uses fuel salt (liquid nuclear fuel). The MSR has been researched and developed extensively at Oak Ridge National Laboratory (ORNL). They not only built and operated a 7.5 MWth MSR experimental reactor but also performed a study of the conceptual design of the molten-salt breeder reactor (MSBR)[1,2]. In Japan, Mitachi et al. studied the MSR for utilizations of Th and Pu from light-water reactors[3,4].

The noteworthy reactor structure of the MSR is that fuel salt circulates inside the reactor during the fission reaction and flows out to the external-loop system composed of a heat exchanger and a circulation pump. Therefore, fuel salt flow decreases the number of delayed neutron precursors in the reactor, and hence affects neutron flux and heat generation distributions. It is necessary to consider the effect of fuel salt flow when we analyze the reactor characteristics and consider the safety precautions of the MSR system. However, in almost all past studies of the MSR, a uniform temperature distribution was assumed in the reactor and fuel salt flow was disregarded. Sides[5] and Shimazu et al.[6] developed MSR analytical models based on the point reactor kinetics model to consider the effect of fuel salt flow. Their models represented a reactor as having six zones for fuel salt and three zones for the graphite moderator. Since their models employed the point reactor kinetics model and the rough temperature approximation, their results were not sufficiently accurate to consider the effect of fuel salt flow correctly or in detail.

In the previous study, the authors developed a new MSR numerical simulation model which can be used to

* Received 8th June, 2005 (No. 04-4151)

** Department of Mechanical Engineering, Toyohashi University of Technology, 1–1 Hibarigaoka, Tenpaku-cho, Toyohashi 441–8580, Japan.
E-mail: taka@mech.tut.ac.jp

estimate the effect of fuel salt flow in detail and performed the analysis of the plug flow field of fuel salt[7),(8)]. The results revealed that fuel salt flow affected the distributions of the precursors significantly, but those of neutron fluxes slightly. We apply the model to the steady-state analysis of the MSR system and simulate the effects of not only fuel flow but also fuel salt inflow temperature and external-loop transit time.

Nomenclature

C_i : number density of i-th delayed neutron precursor, 1/cm^3
c_F : specific heat of fuel salt, J/(g·K)
c_G : specific heat of graphite moderator, J/(g·K)
D : cell diameter, cm
d : equivalent diameter of fuel duct, cm
Fr : volume fraction of fuel salt
k_{eff} : effective neutron multiplication factor
l : length of flow channel, cm
q_F : heat generated in fuel salt, W/(cm^3 of fuel salt)
q_G : heat generated in graphite moderator, W/(cm^3 of graphite moderator)
q_{GF} : heat transfer between fuel salt and graphite moderator, W/cm^3
S : heat transfer area per unit volume, cm^2/cm^3
T_F : fuel salt temperature, K
T_G : graphite moderator temperature, K
u : axial direction velocity of fuel salt, cm/s
w : radial direction velocity of fuel salt, cm/s
β_i : fraction of i-th delayed neutron precursor
ϵ : heat generation per fission reaction, J/fission
ρ_F : density of fuel salt, g/cm^3
ρ_G : density of graphite moderator, g/cm^3
ν : neutron generation per fission reaction, 1/fission
λ_i : decay constant of i-th delayed neutron precursor, 1/s
Σ_{12} : scattering cross section, 1/cm
Σ_{f1} : fission cross section of fast neutron, 1/cm
Σ_{f2} : fission cross section of thermal neutron, 1/cm
Σ_{a1} : absorption cross section of fast neutron, 1/cm
Σ_{a2} : absorption cross section of thermal neutron, 1/cm
τ_{loop} : external-loop transit time, s

2. Small Molten Salt Reactor

2.1 Reactor configuration

Figure 1 shows the small MSR system analyzed in this study and Table 1 lists its main features. This system is 5.4 m in height and 5.2 m in diameter and is composed of four regions: a core, a graphite reflector, a boron carbide absorber and fuel ducts. The core consists of assemblies of graphite hexagonal cylinders each of which has a flow channel for fuel salt. The equivalent diameter of the hexagonal cylinder is 0.2 m, and the flow channel diameter is 10.95 cm. The graphite reflector and the boron carbide absorber consist of assemblies of graphite plates each with a width of 0.2 m. The graphite plates also have a flow channel with a width of 0.4 cm. All these regions are installed in the reactor vessel made of Hastelloy N. The volume fraction Fr in each region is changed to adjust the fission and capture reaction rates: $Fr = 0.3$ in the core, 0.01 in the reflector and the absorber, and 0.9 in the fuel duct. Fuel salt flows into the reactor at the lower entrance, and flows upward through the flow channels in the core and other regions, accompanied by the nuclear fission reaction and temperature increase. Fuel salt flows out the reactor to the external-loop system through the upper vents. The external-loop system consists of a circulation

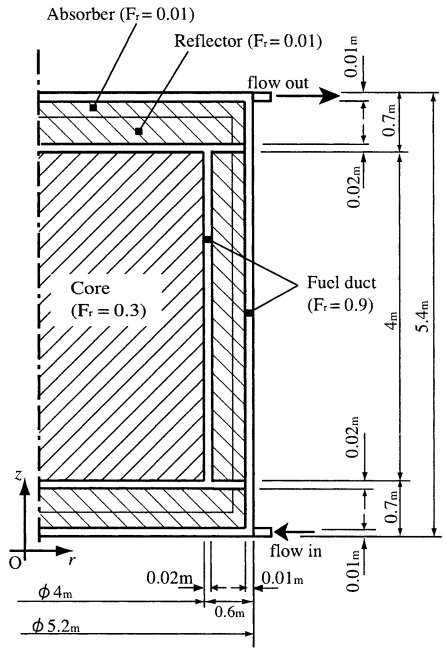

Fig. 1 Schematic drawing of small molten salt reactor

Table 1 Main features of small molten salt reactor

Thermal output (rated power)	350 MW
Fuel salt composition	
LiF	71.78 mol%
BeF_2	16.0
ThF_4	12.0
$^{233}UF_4$	0.22
Fuel salt volume	
Reactor	18.5 m^3
external-loop	4.5 m^3
Graphite volume	96.1 m^3
Fuel salt inflow rate	0.5532 m^3/s
Fuel salt temp. (rated power)	
Inlet	833 K
Outlet	973 K
external-loop transit time, τ_{loop}	8.13 s

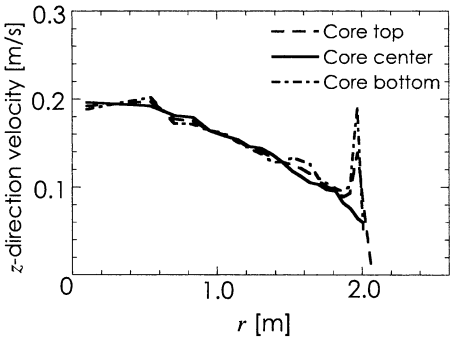

Fig. 2 z-direction velocity distributions of fuel salt (solid line, core center ($z = 2.7$ m); dashed line, core top ($z = 4.7$ m); and dot-dash line, core bottom ($z = 0.7$ m))[7]

pump and heat exchanger. The reactor can operate for a long period due to the continuous reprocessing of fuel.

2.2 Fuel salt flow

In the previous study[3),(4)], the authors performed a nuclear analysis of a small MSR system (shown in Fig. 1) using the neutronics analysis code SRAC (Standard Reactor Analysis Code) developed at the Japan Atomic Energy Research Institute (JAERI). Moreover, computational fluid analysis of fuel salt flow in the MSR was performed in consideration of the heat generation distribution obtained from the SRAC analysis[7]. The calculation conditions were as follows: fuel salt flows into the reactor through lower entrances at a temperature of 833 K and the flow rate of 0.553 2 m^3/s. Then the fuel salt residence time within the reactor was estimated to be approximately 33.4 s. Figure 2 shows the z-direction velocity profiles calculated in the computational fluid analysis: the solid line represents the profile at the core center ($z = 2.7$ m, where z denote a distance from the bottom of the reactor), dashed line is for that at the core top ($z = 4.7$ m), and dot-dash line is for that at the core bottom ($z = 0.7$ m). In the following sections, we discuss the MSR steady state characteristics, referring to these fuel salt velocity profiles.

3. Numerical Model

3.1 Fission reaction

We classify neutron fluxes into two energy groups, fast and thermal neutron fluxes, with the threshold neutron kinetic energy 1.855 eV. Two-group neutron diffusion equations for the fast neutron flux ψ and the thermal neutron flux ϕ are represented as follows[9]:

$$D_1\nabla^2\psi-(\Sigma_{a1}+\Sigma_{12})\psi+(1-\bar{\beta})\frac{v}{k_{eff}}(\Sigma_{f1}+\Sigma_{f2}) +\overline{\lambda C}=0 \quad (1)$$

$$D_2\nabla^2\phi-\Sigma_{a2}\phi+\Sigma_{12}\psi=0, \quad (2)$$

where

$$\nabla^2=\frac{\partial^2}{\partial r^2}+\frac{1}{r}\frac{\partial}{\partial r}+\frac{\partial^2}{\partial z^2}$$

Table 2 Fractions of delayed neutron precursors β_i and decay constants λ_i

Group No.	$\beta_i \times 10^{-4}$, -	λ_i, 1/s
1	2.58	0.0129
2	6.96	0.0347
3	5.46	0.119
4	10.9	0.288
5	3.59	0.805
6	1.26	2.47

$$\bar{\beta}=\sum_{i=1}^{6}\beta_i, \qquad \overline{\lambda C}=\sum_{i=1}^{6}\lambda_i C_i,$$

Delayed neutron precursors are classified into 6 groups according to their half-life periods. The transport equations of the i-th delayed neutron precursor density C_i ($i = 1$–6) is calculated as

$$u\frac{\partial C_i}{\partial r}+w\frac{\partial C_i}{\partial z}=\beta_i\frac{v}{k_{eff}}(\Sigma_{f1}\psi+\Sigma_{f2}\phi)-\lambda_i C_i, \quad (3)$$

where, u and w are radial and axial fuel salt velocities. The effective neutron multiplication factor k_{eff} is defined as

$$k_{eff}=\frac{\iiint(v\Sigma_{f1}\psi+v\Sigma_{f2}\phi)dV}{\iiint(v\Sigma_{a1}\psi+v\Sigma_{a2}\phi)dV-\iint(D_1\nabla\psi+D_2\nabla\phi)dS}, \quad (4)$$

where β_i, v and λ_i denote the fraction of delayed neutron precursors, the neutron production rate and the decay constant, respectively. Detailed data of β_i and λ_i are listed in Table 2.

The nuclear data, fission cross sections Σ_{f1} and Σ_{f2}, absorption cross sections Σ_{a1} and Σ_{a2} and diffusion coefficients D_1 and D_2 depend on fuel salt temperature T_F and graphite moderator temperature T_G. We carried out infinite cell calculations considering the nuclear data including 107 neutron energy groups by means of JENDL3.2 and PIJ (collision probability method code) routine of the SRAC[10]. These cell calculations took into consideration the temperature dependences. The 107 groups of nuclear data obtained in the cell calculations were condensed into two groups of data and consequently used in Eqs. (1)–(4). The boundary conditions for the neutron fluxes ψ and ϕ were set to zero on the inner surface of the reactor vessel. The fuel salt that flows out from the reactor passes through the external-loop system, and subsequently, re-enters the reactor at the bottom. When we defined the external-loop transit time (τ_{loop}), the re-entry density of the delayed neutron precursors, $C_{i,in}$, is derived as

$$C_{i,in}=C_{i,out}\cdot\exp(-\lambda_i\cdot\tau_{loop}). \quad (5)$$

$C_{i,out}$ and λ_i denote the outflow density and the decay constant of delayed neutron precursors, respectively. The external-loop transit time τ_{loop} under the rated operation condition is 8.13 s.

Table 3 Thermal properties of fuel salt and graphite moderator[2]

	Fuel salt	Graphite moderator
ϱ, g/cm^3	Eq.8	1.84
c, J/(g·K)	1.357	1.76
λ, W/(cm·K)	0.012	0.312

3.2 Heat transfer

Fuel salt temperature T_F and graphite moderator temperature T_G are calculated using

$$\rho_F C_F(u\frac{\partial T_F}{\partial r}+w\frac{\partial T_F}{\partial z})=\lambda_F\nabla^2 T_F+q_{\mathrm{F}}+\frac{q_{\mathrm{GF}}}{Fr} \quad (6)$$

$$\lambda_G\nabla^2 T_G+q_{\mathrm{G}}-\frac{q_{\mathrm{GF}}}{1-Fr}=0, \quad (7)$$

where ρ, c and λ denote the density, the specific heat capacity and the specific heat conductivity. Subscripts F and G indicate fuel and graphite, respectively. The fuel salt density depends on the fuel salt temperature and is calculated as

$$\rho_F=3.934-0.668\times10^{-3}T_F. \quad (8)$$

Thermal properties of fuel salt and the graphite moderator are shown in Table 3[2].

For heat generation by the fission reaction, 90% of the fission energy is the kinetic energy of fission fragments and is converted into heat in the fuel salt[11]. The remaining 10% of the fission energy is emitted as the kinetic energy of fast neutrons and γ-ray energy and changes into heat in both the fuel salt and the graphite moderator due to their high permeability. This study takes into account the heat generation mechanism stated here in the calculation of the heat generation by fuel salt and the graphite moderator as follows:

$$q_{\mathrm{F}}=\epsilon(\Sigma_{f1}\psi+\Sigma_{f2}\phi)\left(\frac{0.9}{Fr}+0.1\right) \quad (9)$$

$$q_{\mathrm{G}}=0.1\epsilon(\Sigma_{f1}\psi+\Sigma_{f2}\phi), \quad (10)$$

where ϵ denotes the heat generated per fission reaction. The source term q_{GF} in Eqs. (6) and (7) represents the heat exchange per unit volume between fuel salt and the graphite moderator, and is defined as

$$q_{\mathrm{GF}}=\frac{S}{\left(\frac{1}{h}+\frac{b}{2\lambda_G}\right)}(T_G-T_F). \quad (11)$$

S and b denote the heat transfer area per unit volume and the mean width of the graphite moderator, respectively. Heat transfer coefficient h is derived using Hausen's and Dittus and Boelter's equations[12]:

$$Nu=3.65+\frac{0.066\,8(d/l)Re\cdot Pr}{1+0.04\{(d/l)Re\cdot Pr\}^{2/3}}, Re<2\,300 \quad (12)$$

$$Nu=0.023\cdot Re^{0.8}\cdot Pr^{0.4}, \quad Re\geq2\,300, \quad (13)$$

where Nu, Re and Pr denote the Nusselt, the Reynolds and the Prandtl numbers, respectively. d and l are the equivalent diameter and length of the flow channel of fuel salt. Fuel salt temperature T_F at the entrance is set to equal T_{in}. Boundary conditions of fuel and graphite moderator temperatures are considered to be adiabatic on the inner surface of the reactor vessel. This analysis keeps the thermal output of the small MSR at constant 350 MW. The two-dimensional cylindrical finite difference grid employed here has 64×32 grid nodes in the axial and radial directions. The spatial discretization of the above equations is based on the control volume method[13], and makes use of the central difference method for diffusion terms and the hybrid method for convection terms. The discrete equations are iteratively solved by the SOR (Successive Overrelaxation) algorithm.

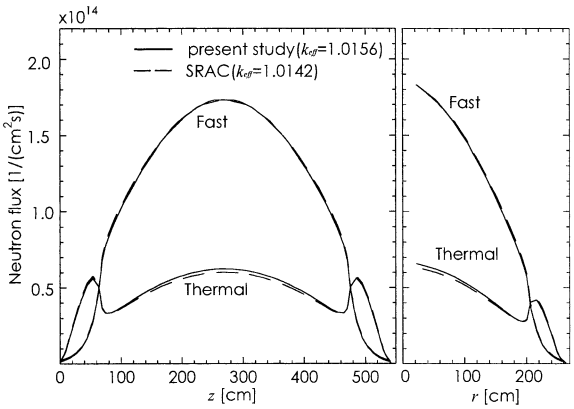

Fig. 3 Neutron flux distributions calculated using the present model and the SRAC ($T_F=T_G=833$ K)

4. Results and Discussion

4.1 Validation and checking of the numerical model

In order to evaluate the precision of the model developed here, we analyzed the reactor characteristics with the assumptions of a uniform temperature ($T_F=T_G=833$ K) and disregarding fuel salt flow ($V_{rate}=0\,\mathrm{m}^3/\mathrm{s}$) and heat generation by the fission reaction. Furthermore the results were compared with the SRAC analysis. For the SRAC analysis, infinite lattice cell analysis was performed using the PIJ routine. Subsequently, the nuclear analysis of the two-dimensional r–z system shown in Fig. 1 was carried out using the two-group cross-sectional data obtained by the PIJ analysis and the CITATION routine in the SRAC. Figure 3 shows neutron flux distributions in axial and radial directions. The results of using the present model (solid line) agree with those of the SRAC analysis (dashed line). The effective neutron multiplication factor k_{eff} is 1.015 6 for the present model, and 1.014 2 for the SRAC. These results lead to conclusion that the analytical model developed here can be used to estimate the nuclear characteristics of a small MSR with a high accuracy comparable to that of the SRAC code.

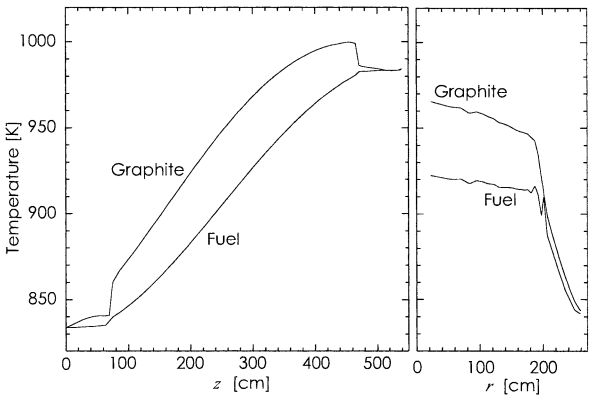

Fig. 4 Temperature distributions of fuel salt and graphite moderator (V_{rate} = 0.553 2 m^3/s, T_{in} = 833 K, τ_{loop} = 8.13 s)

4.2 Fuel salt and graphite moderator temperatures in the rated operation

Figure 4 shows the temperature distributions along the axial and radial directions. These results indicate the consideration of heat generation by both the fission reaction described by Eqs. (9)–(11) and fuel salt flow shown in Fig. 2. That is, the calculation conditions simulate actual rated operation conditions of the small MSR.

The axial fuel salt temperature gradually increases from 833 K at the bottom to 984 K at the upper reflector. The axial graphite moderator temperature increases to the maximum value of 1 000 K at the top of the core (z = 4.7 m), and then decreases to 984 K because of the small amount of heat generated in the reflector and the absorber. Radial fuel salt and graphite moderator temperatures show almost flat distributions in the core.

4.3 Neutron fluxes and delayed neutron precursors distributions in the rated operation

Figure 5 shows the neutron flux distributions in the rated operation condition. The solid lines in Fig. 5 indicate the rated operation conditions when the fuel salt flow shown in Fig. 2 and heat transfer and heat generation by the fission reaction described by Eqs. (9)–(11) were taken into account. The dashed lines represent results obtained assuming uniform temperatures of fuel salt and the graphite moderator ($T_F = T_G$ = 833 K) and disregarding fuel salt flow (V_{rate} = 0.0 m^3/s). The peaks of neutron fluxes at the rated operation move 12 cm toward the bottom from the center of reactor. For the above reasons, the nuclear fission reaction is suppressed in the high-temperature zone at the upper part of the reactor. On the contrary, it is activated in the low-temperature zone at the lower part of the reactor due to the constant power output of 350 MW. In order to clarify the effect of fuel salt flow on neutron flux distributions, the dot-dash lines in Fig. 5 show the results obtained using the temperature distribution in the rated operation disregarding fuel salt flow. On the basis of comparisons of solid lines and dot-dash lines

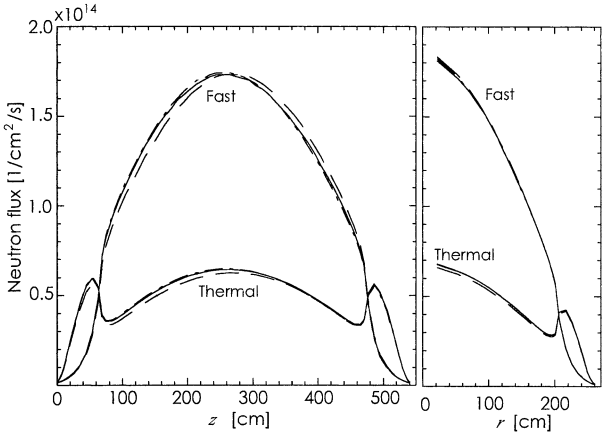

Fig. 5 Effect of fuel salt flow on neutron fluxes (solid line, V_{rate} = 0.553 2 m^3/s, T_{in} = 833 K, τ_{loop} = 8.13 s; dashed line, V_{rate} = 0.0 m^3/s, $T_F = T_G$ = 833 K; and dot-dash line, V_{rate} = 0.553 2 m^3/s, $T_F = T_G$ = rated operation condition)

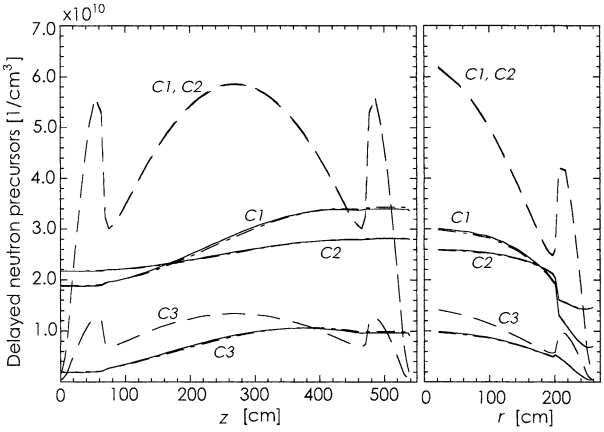

Fig. 6 Effect of fuel salt flow on the 1st – 3rd delayed neutron precursors (solid line, V_{rate} = 0.553 2 m^3/s, T_{in} = 833 K, τ_{loop} = 8.13 s; dashed line, V_{rate} = 0.0 m^3/s, $T_F = T_G$ = 833 K; and dot-dash line, V_{rate} = 0.553 2 m^3/s, $T_F = T_G$ = 833 K, τ_{loop}=8.13 s)

in Fig. 5, it is concluded that the peaks of neutron flux distributions in the rated operation condition slightly move toward the bottom due to the temperature distribution in the reactor rather than fuel salt flow.

The distributions of delayed neutron precursor densities C_i are shown by solid lines in Figs. 6 and 7. For comparison, the results obtained disregarding fuel salt flow (V_{rate} = 0.0 m^3/s) and assuming uniform temperature ($T_F = T_G$ =833 K) are also indicated by dashed lines in the figures. Fuel salt flow carries delayed neutron precursors downstream. As shown in Fig. 2, the z-direction fuel salt velocity w at the center of the core attains approximately 0.2 m/s. Then moving distances of the delayed neutron precursors, which will be reduced by half, can be calculated. The results are shown in Table 4. The distances are 10.7 m in C_1, but 17 cm in C_5 and 6 cm in C_6. On

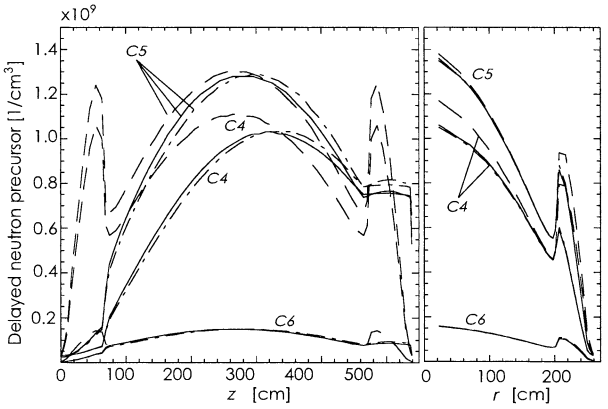

Fig. 7 Effect of fuel salt flow on the 4th – 6th delayed neutron precursors (solid line, $V_{rate} = 0.553\,2\,\mathrm{m^3/s}$, $T_{in} = 833\,\mathrm{K}$, $\tau_{loop} = 8.13\,\mathrm{s}$; dashed line, $V_{rate} = 0.0\,\mathrm{m^3/s}$, $T_F = T_G = 833\,\mathrm{K}$; and dot-dash line, $V_{rate} = 0.553\,2\,\mathrm{m^3/s}$, $T_F = T_G = 833\,\mathrm{K}$, $\tau_{loop} = 8.13\,\mathrm{s}$)

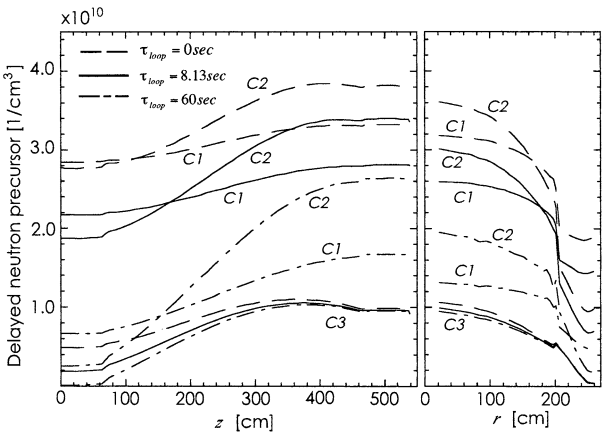

Fig. 8 Effect of external-loop transit time on the 1st – 3rd delayed neutron precursors ($V_{rate} = 0.553\,2\,\mathrm{m^3/s}$, $T_{in} = 833\,\mathrm{K}$)

the other hand, the densities of re-entry delayed neutron precursors $C_{i,in}$ are calculated using Eq. (5). Under this calculation condition, the external-loop transit time τ_{loop} is set at 8.13 s, and consequently, 90% of C_1 flowing out from upper vent re-enters at the bottom of the reactor, and 75% of C_2; on the contrary, almost all of C_5 and C_6 decay in the external-loop system. Therefore, the effect of fuel salt flow strongly appears in the distributions of delayed neutron precursors C_1 and C_2 compared with those of C_5 and C_6. In order to clarify the effect of temperature on the distribution of delayed neutron precursor densities C_i, the results obtained when $V_{rate} = 0.553\,2\,\mathrm{m^3/s}$ and $T_F = T_G = 833\,\mathrm{K}$ are indicated as the dot-dash lines in Figs. 6 and 7. The delayed neutron precursors C_i under the uniform temperature condition move slightly toward the upper region of the reactor compared with the results obtained under the rated operation condition. The main reason is that under the uniform temperature condition, temperatures in the upper part of the reactor are lower than those in the rated operation; consequently, the nuclear fission reaction is activated there. It is noted that the effect of temperature on C_i distribution is weaker than that of fuel salt flow.

In the past study[3,4], the authors designed the outline of the small MSR analyzed in this paper and investigated neutron irradiation damage on graphite moderator and reactor vessel. Furthermore, the authors confirmed that the small MSR designed was able to operate continuously for more than thirty years without the replacement process of graphite moderator. These results stated here (Figs. 5–7) lead that we will be able to directly reflect the reactor design to the construction state of MSR.

4.4 Effect of external-loop transit time on delayed neutron precursors

The external-loop of the MSR consists of a heat exchanger and a fuel salt pump, and its transit time is designed to be 8.13 s in this study. In conventional nuclear reactors such as BWR and PWR, fission fuel does not move in the reactor. On the other hand, fission fuel flows inside the reactor and flows out to the external-loop of the MSR; that is, the number of delayed neutron precursors in the reactor decreases and consequently, the neutron multiplication factor k_{eff} decreases. Therefore, we must clarify the effect of external-loop transit time on the MSR characteristics, even though there is no need to consider this transit time in the conventional nuclear reactors. To evaluate the effect of external-loop transit time on delayed neutron precursors, two cases ($\tau_{loop} = 0$ and 60 s) are additionally examined with heat generation by fission reaction and fuel salt flow ($V_{rate} = 0.553\,2\,\mathrm{m^3/s}$, $T_{in} = 833\,\mathrm{K}$) taken into consideration. For both external-loop transit times, the temperature distributions of fuel salt and the graphite moderator correspond to the results obtained with $\tau_{loop} = 8.13\,\mathrm{s}$ shown in Fig. 3. Furthermore the distributions of fast and thermal neutron fluxes also correspond to the results shown in Fig. 5 where $\tau_{loop} = 8.13\,\mathrm{s}$. The effect of external-loop transit time on temperature and neutron flux is very weak.

Figures 8 and 9 show the effect of external-loop transit time on delayed neutron precursors. The solid lines in Figs. 8 and 9 indicate the results obtained with $\tau_{loop} = 8.13\,\mathrm{s}$, which are the same as the results shown by the solid lines in Figs. 6 and 7. The dashed lines are the results obtained with $\tau_{loop} = 0\,\mathrm{s}$; then all of the delayed neutron precursors, that outflow from the reactor re-enter at the bottom of the reactor. Hence, the number of delayed neutron precursors increases at the bottom. However, the distribution of C_6 changes negligibly due to the very short half-life period. The dot-dash lines are the results obtained with $\tau_{loop} = 60\,\mathrm{s}$. Most of the delayed neutron precursors had decayed in the external-loop (*see* Table 4). Consequently, the density at the bottom of the reactor decreases.

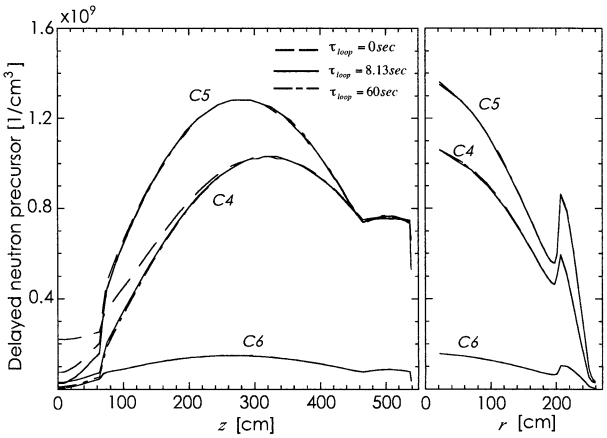

Fig. 9 Effect of external-loop transit time on the 4th – 6th delayed neutron precursors ($V_{rate} = 0.553\,2\ \mathrm{m^3/s}$, $T_{in} = 833\ \mathrm{K}$)

Table 4 Proportions of delayed neutron precursors which re-enter the reactor by escaping decay in the external-loop

Group No.	$0.693 \cdot w/\lambda_i$, m	$C_{i,in}/C_{i,out}$, -	
		$\tau_{loop} = 8.13s$	$\tau_{loop} = 60.0s$
1	10.74	0.90	0.46
2	4.00	0.75	0.12
3	1.17	0.38	0.08
4	0.48	0.10	0.000
5	0.17	0.001	0.000
6	0.06	0.000	0.000

fuel salt velocity w=0.2m

Table 5 Effect of external-loop transit time on neutron multiplication factor

τ_{loop}, s	0	8.13	60
k_{eff}, -	1.0136	1.0134	1.0131

Moreover there is no effect of the external-loop transit time on delayed neutron precursors C_5 and C_6 because of their short half-life periods. It is concluded that the external-loop transit time affects only long-living delayed neutron precursors. Extending external-loop transit time τ_{loop} from 8.13 s to 60 s decreases the neutron multiplication factor by about $0.03\%\Delta k/k$, as listed in Table 5.

4.5 Effect of fuel salt inflow temperature on reactor characteristics

Under the rated operation condition, we considered three fuel salt inflow temperatures (T_{in} = 783 K, 833 K, and 883 K). As a result, the axial and radial distributions of the fuel and graphite temperatures are found to be parallel to the temperature distributions shown in Fig. 4. The fast and thermal neutron fluxes negligibly change, and the delayed neutron precursor densities almost correspond to the results shown by the solid lines in Figs. 6 and 7. Table 6 shows the changes of neutron multiplication factors k_{eff} with fuel inflow temperature. Increasing the fuel inflow temperature by 50 K decreases the neutron multiplication factor by approximately $0.13\%\Delta k/k$. From these results, the temperature coefficient of reactivity α_T of the small MSR is estimated to be -2.7×10^{-5} 1/K.

Table 6 Effect of fuel salt inflow temperature on neutron multiplication factor

T_{in}, K	783	833	883
k_{eff}, -	1.0148	1.0134	1.0121

5. Conclusions

We analyzed the steady-state characteristics of a small molten salt reactor using new numerical model. This model consists of two-group neutron diffusion equations for fast and thermal neutron fluxes, conservation equations for six-group delayed neutron precursors, and energy equations for fuel salt and the graphite moderator. The following results we obtained in this study.

1. In the rated operation condition, the peaks of neutron fluxes move toward the bottom from the center of the reactor due to temperature distributions of fuel salt and graphite moderator.

2. In the results obtained with external-loop transit time τ_{loop} = 8.13 s, 10% of the 1st delayed neutron precursors decay in the external-loop system and 25% of the 2nd delayed neutron precursors. In contrast, almost all 5th and 6th delayed neutron precursors decay in the loop.

3. Extending the external-loop transit time decreases effective multiplication factor k_{eff}; when τ_{loop} increases from 8.13 s to 60 s, multiplication factor k_{eff} decreases by $0.03\%\Delta k/k$.

4. Raising the inflow temperature of fuel salt decreases effective multiplication factor k_{eff}; when inflow temperature T_{in} increases by 50 K from 833 K, effective multiplication factor k_{eff} decreases by approximately $0.13\%\Delta k/k$.

References

(1) Robertson, R.C., Conceptual Design Study of a Single-Fluid Molten Salt Breeder Reactor (ORNL-4541), Oak Ridge National Laboratory, (1970).

(2) Research Committee of Molten Salt Breeder Reactor, Molten Salt Breeder Reactor, Atomic Energy Society of Japan, Tokyo, (1977).

(3) Mitachi, K., Furukawa, K. and Minami, K., Nuclear Characteristics of Small Molten Salt Reactor, (in Japanese), Atomic Energy Society of Japan, Vol.32 (1990), pp.377–384.

(4) Mitachi, K., Furukawa, K., Yamana, Y. and Suzuki, T., Neutronic Examination on Plutonium Transmutation by a Small Molten Salt Reactor, IAEA-TECDOC-840, (1995), pp.183–195.

(5) Sides, W.H., Control Studies of a 1 000 MWe MSBR

(ORNL-TM-2927), Oak Ridge National Laboratory, (1970).
(6) Shimazu, Y., Nuclear Safety Analysis of a Molten Salt Breeder Reactor, Journal of Nuclear Science and Technology, Vol.15 (1978), pp.514–522.
(7) Gonda, S., Mitachi, K., Yamamoto, T., Shimazu, Y. and Suzuki, S., A Study on the Characteristics of Small Molten Salt Reactor, (in Japanese), JSME Tokai Research Meeting, JSME Eds., Vol.2 (2002), pp.127–128.
(8) Mitachi, K., Yamamoto, T., Gonda, S., Suzuki, T. and Okumura, Y., Reactor Characteristics of Molten Salt Reactor: An Approach of Solution Considering the Effect of Fuel Salt Flow, (in Japanese), Journal of Atomic Energy Society of Japan, Vol.2 (2003), pp.37–46.
(9) Lamarsh, J.R., Introduction to Nuclear Engineering, (1975), Wesley, NY.
(10) Okumura, K., SRAC: The Comprehensive Neutronics Calculation Code System (JAERI-Data/Code 96-015), Japan Atomic Energy Research Institute, (1996).
(11) Yamamoto, K. and Ishimori, T., Summary of Nuclear Engineering, (1997), Baifukan, Tokyo.
(12) JSME, JSME Data Book: Heat Transfer, 3rd Edition, (1978), JSME, Tokyo.
(13) Patankar, S.V., Numerical Heat Transfer and Fluid Flow, (1980), MacGraw-Hill, NY.